Journal of
Materials Chemistry C

PAPER

View Article Online
View Journal | View Issue

Cite this: J. Mater. Chem. C, 2015, 3, 7878

A large spin-crossover $[Fe_4L_4]^{8+}$ tetrahedral cage†‡

Li Li,[a] Naoto Saigo,[b] Yingjie Zhang,[c] Daniel J. Fanna,[a] Nicholas D. Shepherd,[a] Jack K. Clegg,[d] Rongkun Zheng,[e] Shinya Hayami,[b] Leonard F. Lindoy,[f] Janice R. Aldrich-Wright,[a] Chun-Guang Li,[a] Jason K. Reynolds,[a] David G. Harman[gh] and Feng Li*[a]

Received 8th April 2015,
Accepted 20th May 2015

DOI: 10.1039/c5tc00991j

www.rsc.org/MaterialsC

A large discrete face-capped tetranuclear iron(II) cage, $[Fe_4\mathbf{L}_4](BF_4)_8{\cdot}n$(solvent), was synthesised *via* metal-ion directed self-assembly. The cage is formed from a rigid tritopic ligand that incorporates chelating imidazole-imine functional groups. The cage displays temperature induced spin-crossover and LIESST effects and is amongst the largest iron(II) tetrahedral cages with such properties reported. The synthesis, structure and magnetic properties of this new metallo-cage are presented.

Introduction

Polynuclear Fe(II) coordination cages have received considerable attention and have been demonstrated to display interesting host–guest chemistry[1–7] due to the presence of their well-defined central cavities. The vast majority of these systems have been designed such that their Fe(II) centres are in the low-spin (LS) state at ambient temperatures; there are only a few examples of Fe(II) cages that show spin-crossover (SCO) or high-spin (HS) behaviour.[8–12] The successful construction of larger supramolecular Fe(II) cages, especially those containing spin-crossover Fe(II) centres, still remains a challenge. Clearly the design of the organic ligand is a key element for achieving such SCO molecular cage systems.

In the present study, building on design principles demonstrated to be successful by Kruger,[11] Nitschke[10] and Gu;[8] imidazole-imine sites were included in the organic ligand component since these groups show weaker ligand strength than the 2,2′-bipyridyl and pyridyl-imine sites commonly employed in tetrahedral cage syntheses. In addition, imidazole-imine groups have been well documented to be 'classical' coordination units for inducing SCO behaviour in Fe(II) complex systems,[13–18] including the limited number of Fe(II) SCO tetrahedral cages already reported.[8,10,11]

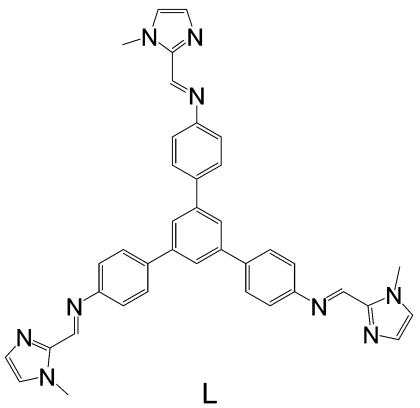

L

Fig. 1 Schematic representation of rigid ligand **L**.

Here we report the synthesis of a new face-capped tetranuclear cage **1** of type $[Fe_4\mathbf{L}_4](BF_4)_8$, employing a large fully conjugated rigid tribranched framework ligand (**L** in Fig. 1) aimed at inducing Fe(II) spin-crossover behaviour at each of its equivalent metal centres.

Results and discussion

The reaction of 1-methyl-2-imidazolecarboxaldehyde and 1,3,5-tris(4-aminophenyl)-benzene in methanol produced the desired C_3-symmetric tris-bidentate ligand **L** in 75% yield. ^{1}H and ^{13}C NMR

[a] School of Science and Health, University of Western Sydney, Penrith, NSW 2751, Australia. E-mail: feng.li@uws.edu.au
[b] Department of Chemistry, Graduate School of Science and Technology, Kumamoto University, 2-39-1 Kurokami, Chuo-ku, Japan
[c] Australian Nuclear Science and Technology Organisation, Locked Bag 2001 Kirrawee DC, NSW 2232, Australia
[d] School of Chemistry and Molecular Biosciences, The University of Queensland, Brisbane St Lucia, QLD 4072, Australia
[e] School of Physics, The University of Sydney, NSW 2006, Australia
[f] School of Chemistry, The University of Sydney, NSW 2006, Australia
[g] Molecular Medicine Research Group, School of Medicine, University of Western Sydney, Building 30, Goldsmith Avenue, Campbelltown, NSW 2560, Australia
[h] Office of the Deputy Vice-Chancellor (Research and Development), University of Western Sydney, Penrith, NSW 2751, Australia

† The themed issue on 'Spin-State switches in Molecular Materials Chemistry'.

‡ Electronic supplementary information (ESI) available: NMR, ESI-Mass, FT-IR and Raman spectra and TGA. CCDC 1057843. For ESI and crystallographic data in CIF or other electronic format see DOI: 10.1039/c5tc00991j

spectra (Fig. S1 and S2, ESI‡) and high resolution electrospray ionisation (HR-ESI) mass spectrometry results were consistent with the proposed structure of **L**. In the HR-mass spectrum, the major peak is observed at *m*/*z* 628.2943 $[\mathbf{L} + H]^+$ (Fig. S3, ESI‡) and the appropriate isotope pattern for $[\mathbf{L} + H]^+$ was observed (Fig. S4, ESI‡).

The further reaction of **L** with iron(II) tetrafluoroborate in acetonitrile followed by the slow diffusion of diethyl ether into the reaction mixture produced prismatic crystals of $[Fe_4\mathbf{L}_4][BF_4]_8 \cdot 16MeCN$ suitable for X-ray diffraction studies (Fig. 2). The four homochiral facially coordinated octahedral metal centres are bridged by four of the ligands such that the ligands cover each face of a tetrahedron, and each tetrahedron has overall *T*-symmetry with C_3-axes of symmetry passing through each metal centre and the centre of each ligand. There are three independent complexes in the asymmetric unit and the iron(II) centres within each tetrahedron are separated by between 14.5 and 15.1 Å placing this amongst the largest spin-crossover cages yet synthesised. For comparison, the two other spin-crossover cages reported have iron–iron separations of 11.85 Å[10] and 14.16.[11] Unlike many related complexes, this coordination cage crystallises in a chiral space group (*P*3) such that the cage molecules spontaneously resolve within each crystal. In the crystal examined all the metal centres displayed *Δ*-stereochemistry. The cage encapsulates a volume of 183 Å^3 [19] and no significant residual electron density was located within the central cavity. The iron–nitrogen bond lengths are between 1.961(11) and 2.288(10) Å consistent with the magnetic results which suggest an intermediate spin at 100 K. Attempts to collect a crystal structure of the cage in its high-spin state (300 K) failed due to solvent loss from the crystals. In addition, scanning electron microscopy (SEM) photographs confirmed that the nanocage **1** uniformly crystallised in a polyhedral shape (Fig. 3a–c) and the crystals underwent rapid decay due to the loss of solvents (Fig. 3b and c).

Elemental analysis of the tetrahedral cage **1** suggested a metal : ligand ratio consistent with the crystal structure. Scanning electron microscopy-energy-dispersive spectroscopy (SEM-EDS) analysis of **1** was also carried out to support the above results. HR-ESI mass spectrometry results (Fig. S5–S12, ESI‡) clearly revealed a series of peaks of various charges corresponding to $[Fe_4\mathbf{L}_4][BF_4]_{(8-n)}^{n+}$ (n = 1–8), which are consistent with the successive loss of $[BF_4]^-$ anions.

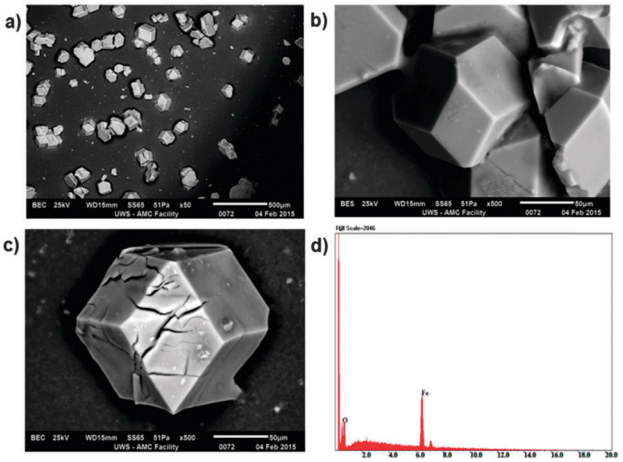

Fig. 3 SEM images of crystals with polyhedral shape (a, b and c) and an EDS spectrum of cage **1** (d).

The UV-vis spectrum of the coordination cage **1** in the solid state over the region 2000–350 nm (Fig. 4) reveals a relative low broad absorption band at 530 nm and an intense band at 410 nm. The former is attributed to a metal-to-ligand (MLCT) (d–π*) transition characteristic of an Fe(II) centre coordinated to a imidazole-imine based large aromatic ligand.[8,11] The intense band at 410 nm is likely to arise from π–π* transitions.[8,11]

FT-IR spectra and Raman spectra of **L** and **1** were recorded at room temperature (Fig. S13, S14 and S15, S16, ESI‡). Both the ligand **L** and coordination cage **1** show absorptions in the region 1600–1500 cm^{-1}, these signals are typical of stretching imidazole-imine (C=N) groups. In the FT-IR spectrum of cage **1** (Fig. S14, ESI‡), it shows the existence of BF_4^- at 1047 cm^{-1}.

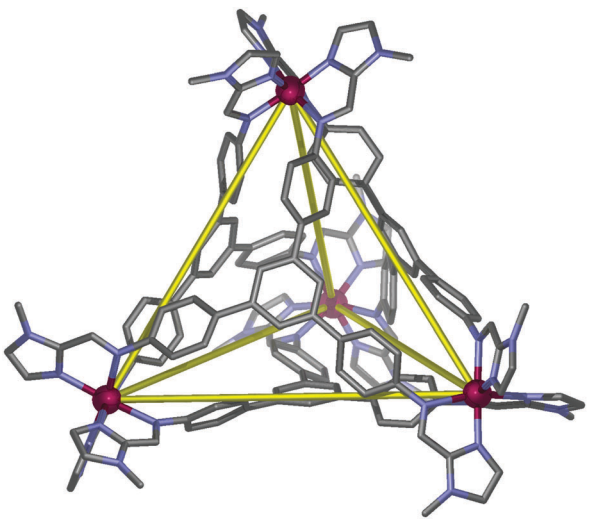

Fig. 2 Schematic representation of the X-ray structure of cage **1**. Hydrogen atoms, anions and solvent molecules are not shown for clarity.

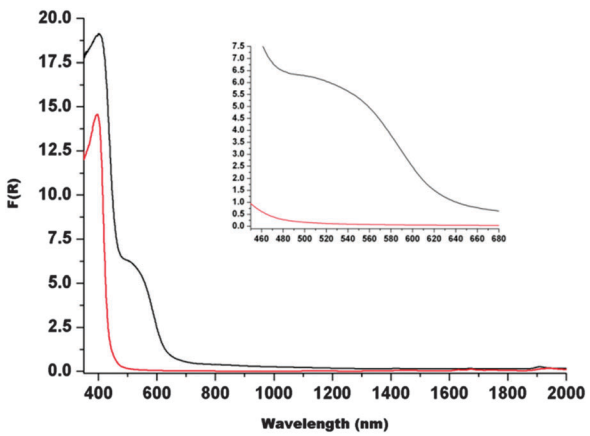

Fig. 4 Solid state UV-vis-NIR spectra (F(R) is the Kubelka-Munk transform) of **L** (red) and **1** (black). The inset shows the relatively low intensity transition in region 450–680 nm.

Raman spectra of **L** (Fig. S15, ESI‡) and **1** (Fig. S16, ESI‡) are very similar and also confirmed the presence of C═N groups.

Magnetic measurements

Magnetic susceptibility measurements reveal a gradual incomplete spin transition over the range 5–300 K (Fig. 5). The spin-crossover phenomenon between the high-spin and low-spin states for solvated $[Fe_4\mathbf{L}_4](BF_4)_8{\cdot}16CH_3CN$ and non-solvated $[Fe_4\mathbf{L}_4](BF_4)_8$ was followed by measurements of the molar magnetic susceptibility χ_m as a function of temperature (Fig. 5a and b).

The χ_mT value for $[Fe_4\mathbf{L}_4](BF_4)_8{\cdot}16CH_3CN$ is equal to 11.44 cm^3 K mol^{-1} at 300 K and 7.85 cm^3 K mol^{-1} at 50 K consistent with a gradual spin-crossover transition (Fig. 5a). After annealing at 400 K, non-solvated compound $[Fe_4\mathbf{L}_4](BF_4)_8$ was obtained. The χ_mT value of the desolvated material is equal to 11.60 cm^3 K mol^{-1} at 400 K, suggesting iron(II) is in the high-spin state. On cooling, the χ_mT values gradually decreases (Fig. 5b). The χ_mT value at 50 K is equal to 8.29 cm^3 K mol^{-1}, which shows that spin-crossover from the high-spin to the low-spin states is induced in about 30% of the iron(II) ions. In addition, the Mössbauer spectrum measured at 5 K support the existence of iron(II) both in the high-spin and low-spin states (Fig. 6). The χ_mT values are also in agreement with the area ratios of Mössbauer absorption intensity of the high-spin and low-spin species.

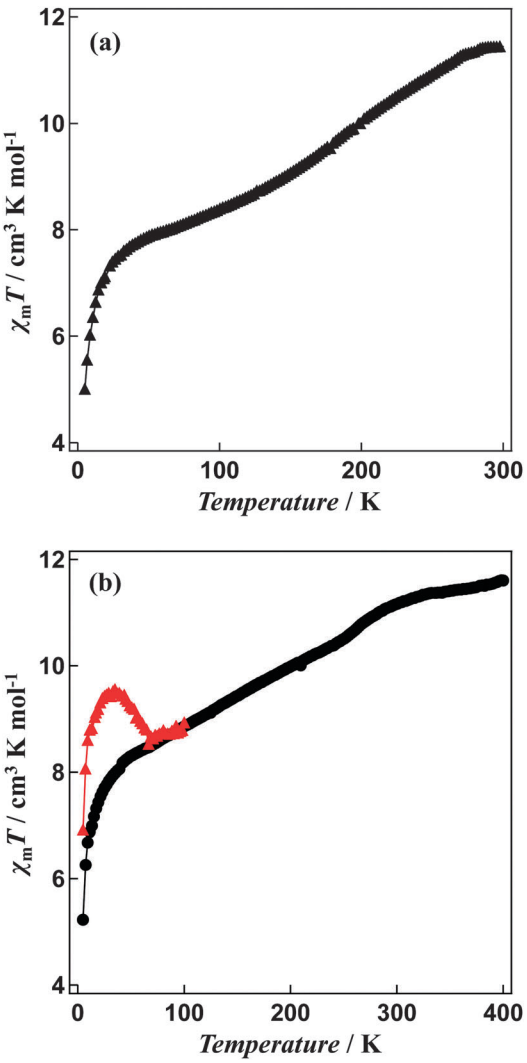

Fig. 5 χ_mT *versus* T plots for (a) solvated $[Fe_4\mathbf{L}_4](BF_4)_8{\cdot}16CH_3CN$, the sample was measured in the temperature range between 5 K and 300 K and (b) non-solvated $[Fe_4\mathbf{L}_4](BF_4)_8$ compound, the magnetic susceptibilities of the sample annealed at 400 K in the SQUID cavity was measured in the temperature range between 5 K and 400 K. χ_mT *versus* T plots for LIESST experiment were recorded in the warming mode after the sample was exposed to light illumination for 1 hour at 5 K.

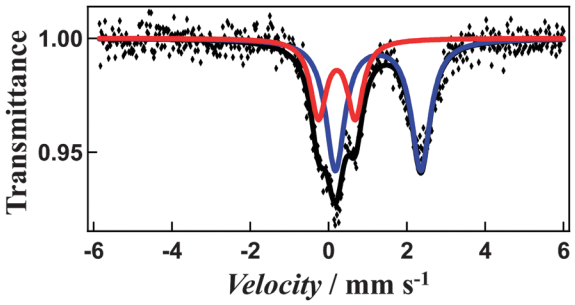

Fig. 6 Mössbauer spectrum of non-solvated cage 1 at 5 K. The iron(II) high-spin is shown in blue, and low-spin in red.

The Mössbauer spectrum measured at 5 K reveals a two quadrupole-split doublets. The first doublet is wide (quadrupole-splitting Q.S. = 2.18 mm s^{-1} and isomer shift I.S. = 1.26 mm s^{-1}) and the second narrow (Q.S. = 0.94 mm s^{-1} and I.S. = 0.21 mm s^{-1}), representing the high-spin and low-spin states (Fig. 6), respectively. The χ_mT values are also in agreement with the area ratios of Mössbauer absorption intensity of the high-spin and low-spin species (67 : 33). This, combined with the magnetic susceptibility studies suggests that the spin transition arises from only one of the four metal centres changing from high-spin to low-spin, while similar cage molecules showed a more complete transition, with three of the four centres switching spin states, potentially arising from changes in metal–metal distances and coordinating ligands.[10,11]

A green semiconductor laser (λ = 532 nm, 10 mW cm^{-2}) was used as a light source to investigate the effects of illumination. The passed light was guided *via* an optical fibre into the SQUID. The sample was placed on the edge of the optical fibre. When the annealed samples were illuminated at 5 K, an increase in the susceptibility by illumination was observed (Fig. 5b). The change in the χ_mT value persisted for several hours, even after the illumination was halted. This suggests that the transition from the low-spin state to the high-spin state can be induced by illumination *i.e.* Light-Induced Excited Spin-State Trapping (LIESST).[20] The χ_mT value decreases with the increase in temperature and that the thermal relaxation to the ground state occurs. The LIESST effect in the non-solvated compound occurs with T(LIESST) of 55 K.

Conclusions

In summary, we describe the efficient synthesis of a new discrete tetranuclear SCO Fe(II) cage incorporating rigid tris-bidentate

ligands with suitable ligand strength arising from the imidazole-imine functional units. The structure has been unambiguously characterised by X-ray crystallography, ESI mass spectrometry, UV-vis-NIR, FT-IR and Raman spectroscopy. SCO behaviour of the coordination cage **1** has been investigated. Further studies on these and related other Fe(II) coordination cages, including a high pressure solid state investigation, are ongoing and will be reported in due course.

Experimental

Materials and synthesis

All reagents and solvents were purchased from commercial sources.

Physical measurements

^{1}H NMR and ^{13}C NMR spectra were recorded on a Bruker 300 MHz spectrometer. High resolution ESI-MS data were acquired using a Waters Xevo QToF mass spectrometer, operating in positive ion mode. FT-IR spectra were recorded on a Bruker Tensor 27 Fourier transform infrared spectrometer using diamond single bounce ATR sampling device. The UV-vis spectra were measured at ambient temperature using a Cary 5000 spectrophotometer equipped with a Labsphere Biconical Accessory.

SEM measurements. The SEM experiments were carried out using SEM JEOL JSM 6510LV with an attached silicon drift EDS detector and operated in low-vac with a chamber pressure of 30 pa. Accelerating voltage was set to 25.0 KV and a spot size of 60.

Raman measurements. Raman spectra were recorded using a Bruker Raman Scope in combination with Senterra dispersive Raman Microscope. The 532 nm line of a laser (0.2 mW for **L** and 2 mW for cage **1**) was used as the excitation source.

Magnetic measurements. Susceptibility data were collected using a Quantum Design SQUID magnetometer calibrated against a standard palladium sample. The data were collected between 5 and 400 K and the scan rate of the temperature was fixed at 2.0 K min^{-1}.

Mössbauer experiments were carried out using a Wissel MVT-1000 Mössbauer spectrometer with a ^{57}Co/Rh source in a constant-acceleration transmission spectrometer (Topologic Systems) equipped with a closed-cycle helium refrigerator cryostat (Iwatani Co., Ltd). All isomer shifts are given relative to α-Fe at room temperature. Measurements at low temperature were performed.

Ligand synthesis

1-Methyl-2-imidazolecarboxaldehyde (469 mg, 4.26 mmol) in methanol (20 mL) was added dropwise to a suspension of 1,3,5-tris(4-aminophenyl)-benzene (500 mg, 1.42 mmol) in methanol (50 mL). The mixture was heated at reflux for overnight leading to a clear yellow solution. The residue obtained after the removal of the solvent was recrystallised from an ethanol–acetonitrile mixture. The crystalline product was washed with acetonitrile (3 × 5 mL) to give **L** as a pale yellow powder (669 mg, 75%). ^{1}H NMR (DMSO, 300 MHz) δ (ppm) 8.59 (s, 3H, aromatic ring), 7.95 (d, 9H, aromatic ring), 7.44 (d, 9H, aromatic ring), 7.19 (s, 3H), 4.09 (s, 9H, methyl); ^{13}C NMR (DMSO, 75.5 MHz) δ (ppm) 151.21, 150.34,142.78, 141.04, 138.01, 129.80, 128.07, 126.61, 123.87, 121.62, 35.24 (–CH_3); FT-IR ATR ν_{max}/cm^{-1}: 3340(br), 1628s, 1594s, 1475s, 873s, 833s, 752s, 688s, 541m; ESI-HRMS (positive-ion detection, CH_3OH/H_2O): m/z = 628.2943.

Complex synthesis

$[Fe_4L_4][BF_4]_8\cdot 28H_2O$. $Fe(BF_4)_2\cdot 6H_2O$ (115 mg, 0.34 mmol) in acetonitrile (10 mL) was slowly added to a mixture of **L** (200 mg, 0.32 mmol) in acetonitrile (50 mL), there was a immediate colour change from yellow to dark red. The reaction mixture was heated on 70 °C with stirring for 4 h. Slow diffusion of diethyl ether into the mixture resulted in the formation of dark red polyhedral crystals and air dry. Yield: 91%. Elemental analysis (%) calcd for $C_{156}H_{188}B_8F_{32}Fe_4N_{36}O_{28}$: C 47.64, H 4.82, N 12.82; found: C 47.51, H 4.77, N 12.88. Single crystals were taken from the same sample and used directly in the X-ray study. FTIR (cm^{-1}): 3392(br), 1597m, 1488m, 1439s, 1292m, 1048s, 965m, 902m, 838m, 777m, 665m, 521w; ESI-HRMS (positive-ion detection, CH_3CN): m/z = 3341.9717 $[Fe_4L_4][BF_4]_7^{+}$; 1627.5011 $[Fe_4L_4][BF_4]_6^{2+}$; 1055.9874 $[Fe_4L_4][BF_4]_5^{3+}$; 770.5002 $[Fe_4L_4][BF_4]_4^{4+}$; 598.9991 $[Fe_4L_4][BF_4]_3^{5+}$; 484.6590 $[Fe_4L_4][BF_4]_2^{6+}$; 402.9929 $[Fe_4L_4][BF_4]^{7+}$; 341.7446 $[Fe_4L_4]^{8+}$.

Crystallography

X-ray structural data were collected at beamline MX1 of the Australian Synchrotron employing silicon double crystal monochromated synchrotron radiation (0.7108 Å) at 100(2) K.[21,22] Data integration and reduction were undertaken with XDS[23] and subsequent computations were carried out using the WinGX-32 graphical user interface.[24] The structure was solved by charge flipping using SUPERFLIP.[25] Empirical absorption corrections were applied to the data set using the program SADABS[26] Data were refined and extended with SHELXL-2014.[27] In general non-hydrogen atoms with occupancies greater than 0.5 were refined anisotropically. Carbon-bound hydrogen atoms were included in idealised positions and refined using a riding model. The crystals employed rapidly lost solvent after removal from the mother liquor. Rapid (<10 seconds) handling at dry ice temperatures prior to quenching in the cryostream was required to collect data. Despite these measures, the use of a synchrotron source and multiple collection attempts, no reflections at better than 0.9 Å resolution were observed. In addition, data collection at the beamline was restricted to a 360° rotation around a single axis resulting in less than ideal redundancy. Reflecting the less than ideal diffraction, there is substantial disorder in a number of the anions which required the use of bond length and angle restraints to facilitate realistic modelling. Further reflecting the solvent loss and poor diffraction properties, there is a significant amount of void volume in the lattice containing smeared electron density from disordered solvent and anions. This area of density could not be successfully modelled and the SQUEEZE[28] function of PLATON[29] was employed resulting in significantly improved residuals. Despite these limitations the quality of the data is more than suitable for

establishing the connectivity of the system. The Flack parameter refined to 0.05(3).[30–33]

Formula $C_{188}H_{180}B_8F_{32}Fe_4N_{52}$, M 4085.71, trigonal, space group *P*3(#143), *a* 31.590(5) Å, *b* 31.590(5) Å, *c* 18.320(4) Å, γ 120°, *V* 15833(6) Å^3, D_c 1.286 g cm^{-3}, *Z* 3, crystal size 0.05 by 0.05 by 0.05 mm, colour orange, habit prism, temperature 100(2) K, λ(Synchrotron) 0.7108 Å, μ(Synchrotron) 0.359 mm^{-1}, $T(\mathrm{SADABS})_{\mathrm{min,max}}$ 0.3657, 0.4272, $2\theta_{\max}$ 43.93, *hkl* range −33 33, −33 33, −19 19, *N* 139 384, N_{ind} 25 723 (R_{merge} 0.0847), N_{obs} 23244($I > 2\sigma(I)$), N_{var} 2204, residuals $R_1(F)$ 0.0961, w$R_2(F^2)$ 0.2580, GoF(all) 1.077, $\Delta\rho_{\mathrm{min,max}}$ −0.579, 1.767 e$^-$ Å^{-3}.

Acknowledgements

The research described herein was supported by the University of Western Sydney (UWS). The authors acknowledge AMCF and MS facilities at UWS and MX1 beamline at the Australian Synchrotron. J.K.C., R.Z. and L.F.L. thank the Australian Research Council for support. L.L. also acknowledges receipt of an Australian Postgraduate Award and UWS Top-up Award.

Notes and references

1 D. M. Wood, W. Meng, T. K. Ronson, A. R. Stefankiewicz, J. K. M. Sanders and J. R. Nitschke, *Angew. Chem., Int. Ed.*, 2015, **54**, 3988–3992.
2 W. J. Ramsay and J. R. Nitschke, *J. Am. Chem. Soc.*, 2014, **136**, 7038–7043.
3 A. Jiménez, R. A. Bilbeisi, T. K. Ronson, S. Zarra, C. Woodhead and J. R. Nitschke, *Angew. Chem., Int. Ed.*, 2014, **53**, 4556–4560.
4 M. M. J. Smulders, S. Zarra and J. R. Nitschke, *J. Am. Chem. Soc.*, 2013, **135**, 7039.
5 P. Mal, B. Breiner, K. Rissanen and J. R. Nitschke, *Science*, 2009, **324**, 1697–1699.
6 C. R. K. Glasson, J. K. Clegg, J. C. McMurtrie, G. V. Meehan, L. F. Lindoy, C. A. Motti, B. Moubaraki, K. S. Murray and J. D. Cashion, *Chem. Sci.*, 2011, **2**, 540–543.
7 C. R. K. Glasson, G. V. Meehan, J. K. Clegg, L. F. Lindoy, P. Turner, M. B. Duriska and R. Willis, *Chem. Commun.*, 2008, 1190–1192.
8 D.-H. Ren, D. Qiu, C.-Y. Pang, Z. Li and Z.-G. Gu, *Chem. Commun.*, 2015, **51**, 788–791.
9 F. Li, N. F. Sciortino, J. K. Clegg, S. M. Neville and C. J. Kepert, *Aust. J. Chem.*, 2014, **67**, 1625–1628.
10 R. A. Bilbeisi, S. Zarra, H. L. C. Feltham, G. N. L. Jameson, J. K. Clegg, S. Brooker and J. R. Nitschke, *Chem. – Eur. J.*, 2013, **19**, 8058–8062.
11 A. Ferguson, M. A. Squire, D. Siretanu, D. Mitcov, C. Mathoniere, R. Clerac and P. E. Kruger, *Chem. Commun.*, 2013, **49**, 1597–1599.
12 M. B. Duriska, S. M. Neville, B. Moubaraki, J. D. Cashion, G. J. Halder, K. W. Chapman, C. Balde, J.-F. Letard, K. S. Murray, C. J. Kepert and S. R. Batten, *Angew. Chem., Int. Ed.*, 2009, **48**, 2549–2552.
13 Y. Sunatsuki, R. Kawamoto, K. Fujita, H. Maruyama, T. Suzuki, H. Ishida, M. Kojima, S. Iijima and N. Matsumoto, *Coord. Chem. Rev.*, 2010, **254**, 1871–1881.
14 N. Bréfuel, H. Watanabe, L. Toupet, J. Come, N. Matsumoto, E. Collet, K. Tanaka and J.-P. Tuchagues, *Angew. Chem., Int. Ed.*, 2009, **48**, 9304–9307.
15 D. Pelleteret, R. Clerac, C. Mathoniere, E. Harte, W. Schmitt and P. E. Kruger, *Chem. Commun.*, 2009, 221–223.
16 N. Brefuel, C. Duhayon, S. Shova and J.-P. Tuchagues, *Chem. Commun.*, 2007, 5223–5225.
17 Y. Sunatsuki, Y. Ikuta, N. Matsumoto, H. Ohta, M. Kojima, S. Iijima, S. Hayami, Y. Maeda, S. Kaizaki, F. Dahan and J.-P. Tuchagues, *Angew. Chem., Int. Ed.*, 2003, **42**, 1614–1618.
18 I. Katsuki, Y. Motoda, Y. Sunatsuki, N. Matsumoto, T. Nakashima and M. Kojima, *J. Am. Chem. Soc.*, 2002, **124**, 629–640.
19 G. J. Kleywegt and T. A. Jones, *Acta Crystallogr., Sect. D: Biol. Crystallogr.*, 1994, **50**, 178–185.
20 J.-F. Létard, L. Capes, G. Chastanet, N. Moliner, S. Létard, J.-A. Real and O. Kahn, *Chem. Phys. Lett.*, 1999, **313**, 115–120.
21 T. M. McPhillips, S. E. McPhillips, H.-J. Chiu, A. E. Cohen, A. M. Deacon, P. J. Ellis, E. Garman, A. Gonzalez, N. K. Sauter, R. P. Phizackerley, S. M. Soltis and P. Kuhn, *J. Synchrotron Radiat.*, 2002, **9**, 401–406.
22 N. P. Cowieson, D. Aragao, M. Clift, D. J. Ericsson, C. Gee, S. J. Harrop, N. Mudie, S. Panjikar, J. R. Price, A. Riboldi-Tunnicliffe, R. Williamson and T. Caradoc-Davies, *J. Synchrotron Radiat.*, 2015, **22**, 187–190.
23 W. Kabsch, *J. Appl. Crystallogr.*, 1993, **26**, 795–800.
24 L. Farrugia, *J. Appl. Crystallogr.*, 1999, **32**, 837–838.
25 L. Palatinus and G. Chapuis, *J. Appl. Crystallogr.*, 2007, **40**, 786–790.
26 G. M. Sheldrick, *SADABS: Empirical Absorption and Correction Software, 1996-2008*, University of Göttingen, Germany, 1996–2008.
27 G. M. Sheldrick, *SHELXS 2014, Program for the solution of crystal structures*, University of Göttingen, Germany, 2014.
28 P. van der Sluis and A. L. Spek, *Acta Crystallogr., Sect. A: Found. Crystallogr.*, 1990, **46**, 194–201.
29 A. Spek, *Acta Crystallogr., Sect. D: Biol. Crystallogr.*, 2009, **65**, 148–155.
30 H. D. Flack and G. Bernardinelli, *J. Appl. Crystallogr.*, 2000, **33**, 1143–1148.
31 H. D. Flack and G. Bernardinelli, *Acta Crystallogr., Sect. A: Found. Crystallogr.*, 1999, **55**, 908–915.
32 G. Bernardinelli and H. D. Flack, *Acta Crystallogr., Sect. A: Found. Crystallogr.*, 1985, **41**, 500–511.
33 H. Flack, *Acta Crystallogr., Sect. A: Found. Crystallogr.*, 1983, **39**, 876–881.

